We are IntechOpen, the world's leading publisher of Open Access books Built by scientists, for scientists

4,800
Open access books available

122,000
International authors and editors

135M
Downloads

Our authors are among the

154
Countries delivered to

TOP 1%
most cited scientists

12.2%
Contributors from top 500 universities

CLARIVATE ANALYTICS BOOK CITATION INDEX INDEXED

WEB OF SCIENCE™

Selection of our books indexed in the Book Citation Index in Web of Science™ Core Collection (BKCI)

Interested in publishing with us?
Contact book.department@intechopen.com

Numbers displayed above are based on latest data collected.
For more information visit www.intechopen.com

12

Complex and Flexible Robot Motions by Strand-Muscle Actuators

Masakazu Suzuki
Tokai University
Japan

1. Introduction

Robots are now requested to perform more and more complex tasks such as rescue activities in quite practical environments such as rough terrains. It is necessary for robots to have versatile joints that can flexibly adapt to such task environments and realize complex motions. It is desired to develop small and low cost actuators which can flexibly adapt to task environment. Flexibility in robot joints is especially necessary in the environment where the robots work around humans. The conventional joint mechanism makes the robots structurally complex, then heavy and large, and expensive. In addition it is difficult for them to control joint stiffness in order to handle soft objects or contact human body. Stiffness control by software servomechanism based on the reaction force from the object measured after contact has been actively investigated. But the time lag of servomechanism often results in undesirable response. On the other hand mechanical stiffness control causes no time lag because the stiffness is determined before the contact with work objects. Vertebrates' joints easily realize joint angle control and stiffness control simultaneously by their antagonistic muscles. A wide variety of artificial muscles are being actively investigated (ex. Proc. 2nd Conf. on Artificial Muscles, 2004). McKibben artificial muscle is the most well-known pneumatic actuator and there are many applications including energy efficient low power joint (Linde, 1999). Another type of vertebrate-joint-like actuator developed by the author's group is Strand-Muscle Actuator, StMA (Suzuki et al., 1997). The actuator can adapt to various tasks and environmental changes. The StMAs, having nonlinear elastic characteristics, realize joint angle/stiffness control, even for multi-DOF joints, by antagonistic actuator installation on the joint. In addition the actuator is expected to realize multi-DOF complex and flexible motions with simple mechanism. The joint angle/stiffness control by StMAs has been investigated, and legged walking robots as well as a multi-DOF human-shoulderlike joint, 5 fingered hands have already been developed. This chapter is to introduce the development and application of the StMAs.

The StMA-based joints are suitable for complex and flexible motions in spite of their simple mechanism, and extendable joint mechanism will be possible with them. An StMAbased joint with redundant muscles realizes failure tolerant angle/stiffness control. The effectiveness has already been verified by legged walking robots, 5 fingered hands, and 3-

Source: Climbing & Walking Robots, Towards New Applications, Book edited by Houxiang Zhang,
ISBN 978-3-902613-16-5, pp.546, October 2007, Itech Education and Publishing, Vienna, Austria

DOF joints. The former sections of the chapter describe the characteristics and control scheme of the StMAs. The latter sections are on some applications: One is the realization of springy walk (quick and energy-efficient rhythmical walk) by a 6-legged StMA-based robot (Suzuki & Ichikawa, 2004). Actuator drive pattern optimization with utilizing the actuators' elastic characteristics results in fast and dexterous actions. Another is on online optimal muscle coordination of multi-DOF joints (Suzuki & Mayahara, 2007). For smooth and dexterous motions real-time cooperative muscle tension control is necessary. A method for optimal redundant muscle coordination is proposed, and it is then successfully applied to an StMA-based 3-DOF joint.

2. Strand-Muscle Actuator

In this section the Strand-Muscle Actuator is introduced, where its mechanism and basic characteristics are presented.

2.1 Mechanical composition and drive principle

A Strand-Muscle Actuator (StMA) has a very simple mechanism (Fig.1). It is composed of a motor and a strand muscle that consists of two (or more) muscle fibers. Giving a torsion to the *strand-muscle* by the motor, the muscle contracts. The motor side end is referred to as the actuator's *driving-end*, and the other side is the *effected-end*. The StMA is a kind of artificial muscle that has nonlinear elastic characteristics like mammal's muscles. Various joints are

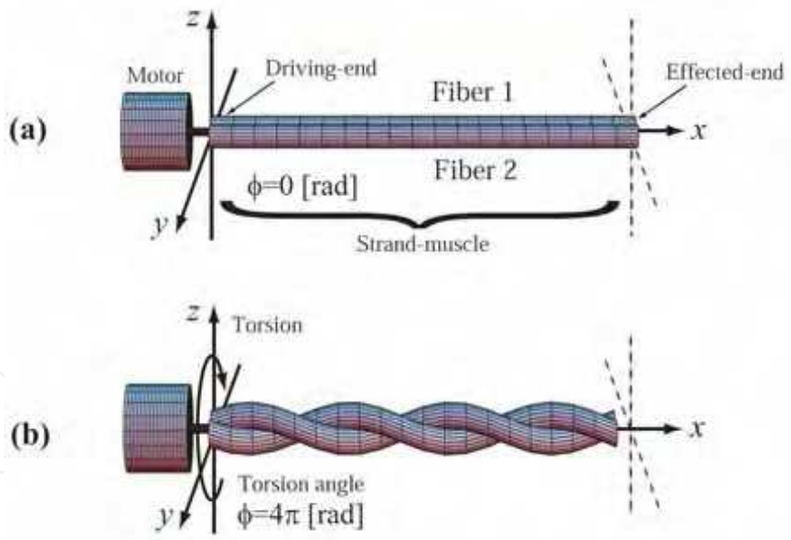

Fig. 1. A Strand-Muscle Actuator with two muscle fibers: (a) natural state and (b) contraction by torsion

realized by antagonistic installation of several StMAs (Fig.2, Fig.9 and Fig.10). In spite of their small size, light weight, and simple mechanism, the StMAs easily realize joint angle/stiffness control. In addition the actuator is expected to realize multi-DOF complex and flexible motions.

Motor and muscle fiber Both DC motors and stepping motors may be used dependingb upon the actuator use. Since a strand-muscle functions as a speed reducer, very small gearless DC motors can be used. And geared DC motors with a small gear ratio are also used to achieve adequate torque and speed with small motors. Stepping motors are convenient for small-step muscle torsion. Therefore the actuator's basic characteristics in subsection 2.2 have been

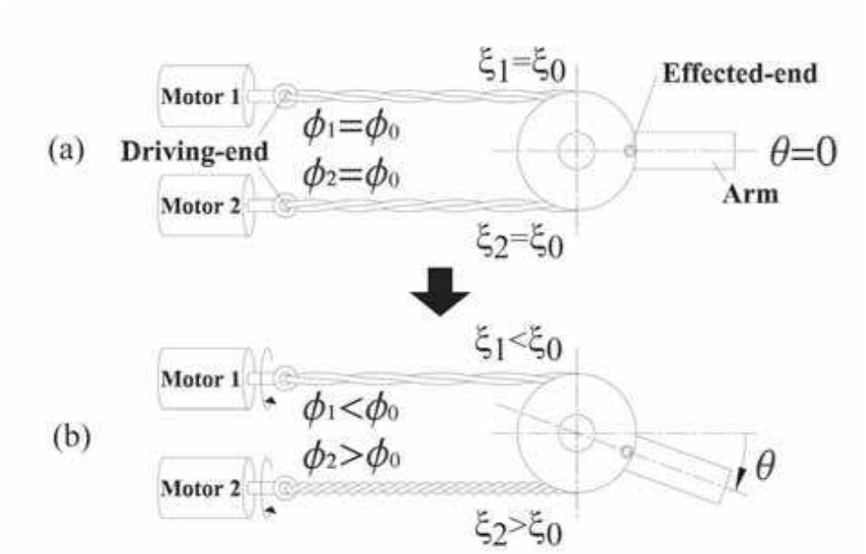

Fig. 2. A pulley-type 1-DOF joint actuated by antagonistic two Strand-Muscle-Actuators

investigated by driving StMAs with stepping motors. Practically, however, all the StMAs for robot joints are presently driven by DC motors in order to make the most use of the StMA's advantages: small, light, simple mechanism.

A muscle fiber of strand-muscle is an elastic thread with circular section. The ideal muscle fiber has elasticity only in the fiber axis direction without diameter change by elongation, no fiber surface friction, no bending stiffness. Actually, however, such ideal characteristics cannot be realized. Various materials such as cotton, wool, nylon, glass fiber, carbon fiber, aramid fiber, silicon rubber and so on have been investigated. At present some kinds of fishing lines such as Flyline (polyester fiber coated with polyvinyl chloride), are used as suitable muscle fiber material.

Contraction by torsion Consider a strand-muscle that consists of two ideal muscle fibers of natural length L and radius r (Fig.3). In the StMA's natural state, the muscle is twistless torsion angle $\phi = 0$, it is not slack, but no tension is exerted (T = 0).

Twisting the fiber strand by angle $\phi > 0$ by the motor the muscle contracts. When the effected-end is free, the muscle length ℓ is determined only by ϕ, and is obtained by a simple geometrical analysis. The locus of the circular section's center of each fiber forms a helix:

$$y = r\cos\frac{\phi}{\ell}x,\ z = r\sin\frac{\phi}{\ell}x\ \ (0 \le x \le \ell)$$

From the fact that the length of the locus is L, the muscle length is obtained as

$$\ell = \sqrt{L^2 - r^2\,\phi^2} \tag{1}$$

From (1) the muscle contraction ξ is then given as

$$\xi = L - \ell = L - \sqrt{L^2 - r^2\phi^2} \tag{2}$$

When the muscle most densely coils, it contracts to $\ell = 4nr$ where n is the number of coil turns. Then, theoretically, the muscle length is $\ell = L/\sqrt{1+\pi^2/4} \simeq 0.537L$, which means the maximum muscle contraction is about 46% of the natural length. Actually, however, the full contraction is difficult to achieve because of uneven twist and large torsion moment. The maximum contraction in practical use is about 30%.

Contraction under tension If the effected-end is not free, the muscle generates tension, say T. This tension is utilized as source of power of the StMA, i.e., StMAs transform rotational torque into linear tensile force. The contraction ξ is then the sum of contraction by torsion $\xi_\phi > 0$ and extension by tension $\xi_T < 0, i.e., \xi = \xi_\phi + \xi_T$. In this situation fiber surface friction and diameter decrease cannot be ignored. The extension by tension has a complicated relation to ϕ, T and fiber material. The relation should thus be experimentally determined.

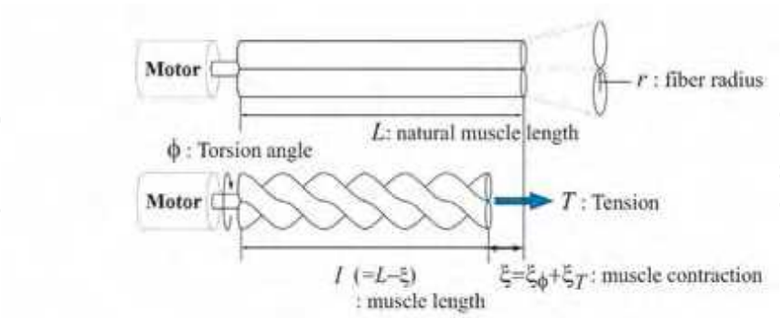

Fig. 3. A Strand-Muscle Actuator in twisted and tense state

2.2 Basic Characteristics

Mechanical characteristics For practical use the relation among the muscle contraction ξ, and the torsion angle ϕ and exerted tension T for a pair of specific muscle fibers should be known and available. Such a relation, $\xi(\phi, T)$, is referred to as the actuator's basic mechanical characteristics or *basic characteristics* in short. The formula $\xi(\phi, T)$ is obtained by motion experiments, and utilized as the control knowledge for StMA control. Note that the characteristics are dependent also on natural length L, fiber radius r and material, though they are not explicitly expressed for simplicity.

The basic characteristics are obtained by measuring ξ under a constant tension T with a device as shown in Fig.4. Increasing and decreasing torsion angles were repeatedly given for 100 times (n = 1, 2 · · · 100) by a stepping motor with sufficient torque. Some typical results for nylon fiber, cotton fiber and Flyline are shown in Fig.5 I, II and III, respectively.

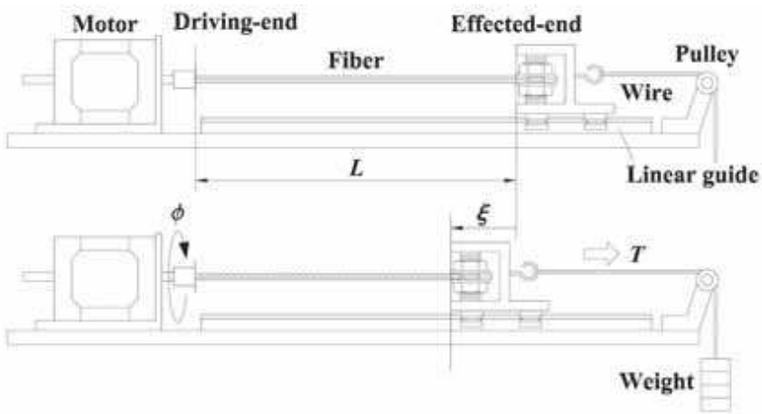

Fig. 4. Experimental device for basic characteristics

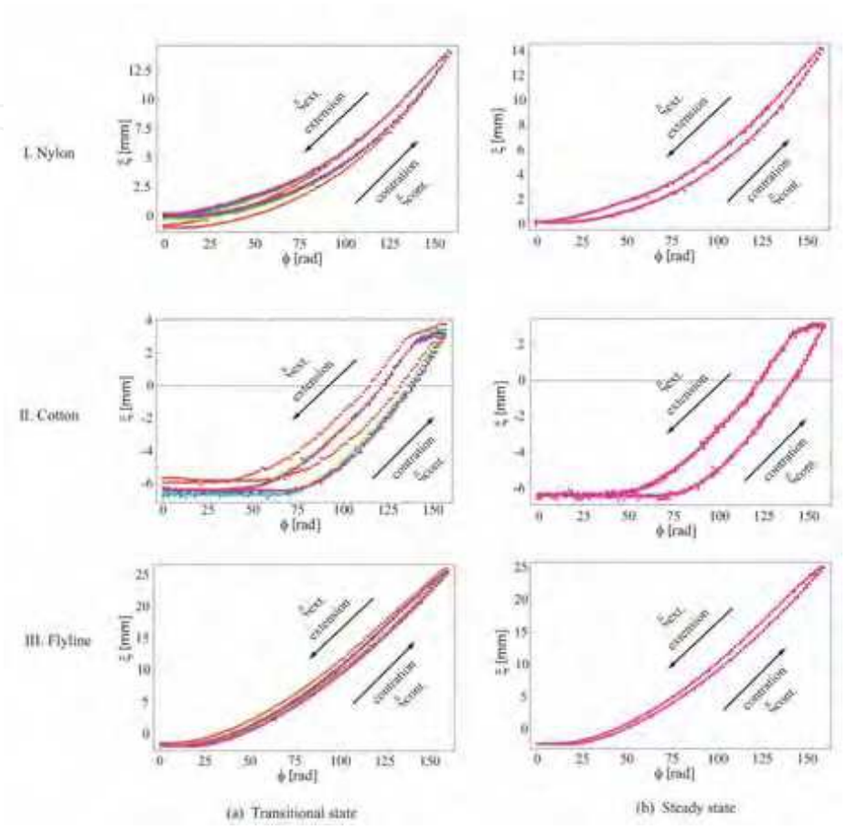

Fig. 5. Basic characteristics of I. nylon, II. cotton, and III. Flyline in (a) transitional state and (b) steady state

The $\phi - \xi$ curves in transitional state (n = 1, 20, 40, 60, 80, 100) gradually change as motions are repeated (Fig.5(a)). Hence some break-in operations are necessary before practical use until the characteristics converge to steady states. Even in the steady state (n = 90 ~ 100), however, they have some hysteresis (Fig.5(b)). Among various materials Flyline has the best characteristics, *i.e.*, least number of necessary break-in operations, highest repeatability and smallest hysteresis error ($\left|\xi_{ext}(\phi,T) - \xi_{cont}(\phi,T)\right|$) which can be negligible for control use.

Based on the result stated above, Flyline has been adopted as the main muscle fiber material, and investigated in detail. The hysteresis error in operation range (usually, $0.05L \le \xi \le 0.25L$) is very small, therefore the contraction/extension average $\frac{1}{2}(\xi_{ext}(\phi,T) - \xi_{cont}(\phi,T))$ was used as the practical basic characteristics for control. Experimental formula of basic characteristics in the form of characteristics in the form of

$$\xi(\phi,T)=\sum_{0\le i+j\le 3} a_{i,j}T^i\phi^j \tag{3}$$

is considered, whose coefficients $a_{i,j}$ were then determined by least mean square approximation. As seen in Fig.6 the measured contraction coincides with the curves by experimental formula very well, and they can be used for practical control with sufficient accuracy. Notethe initial contraction $\xi(0,T)<0$ is caused by the preload tension *T*. The

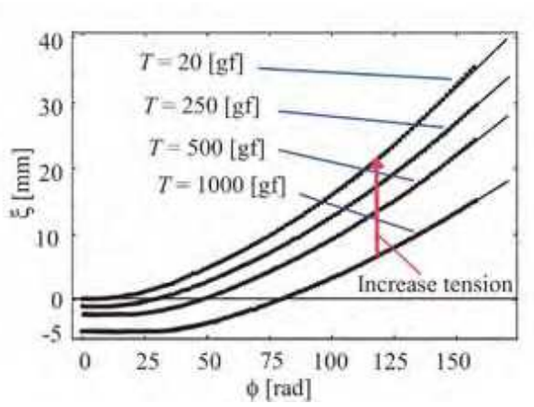

Fig. 6. Experimental formulea of basic characteristics (solid line) and measured muscle contraction (dots) for Flyline

diagram says that twisting the muscle moves the effected-end under constant tension, while it increases the tension when the effected-end is fixed. The 3D expression of the formula (3) is shown in Fig.7.

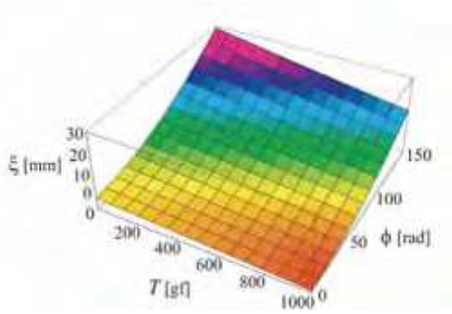

Fig. 7. 3D expression of basic mechanical characteristics $\xi(\phi,T)$ for Flyline

Muscle stiffness The strand-muscles have nonlinear elastic characteristics. Consider muscle stiffness S_M defined as

$$S_M = \frac{\partial T}{\partial \xi} \tag{4}$$

The muscle stiffness $S_M(\phi, T)$ is obtained from (3) by calculating $\left(\frac{\partial \xi(\phi, T)}{\partial T}\right)^{-1}$, which is shown in Fig.8. It should be noted that the muscle is less stiff as the torsion angle increases if the tension is constant.

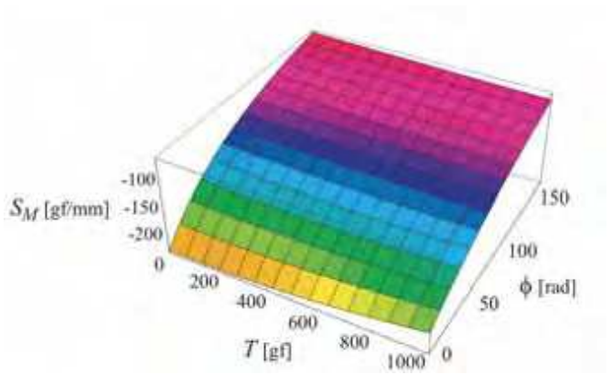

Fig. 8. 3D expression of muscle stiffness $S_M(\phi, T)$

Control characteristics For a complex and flexible robot motion by parallely installed many elastic muscles, simple open-loop on/off muscle control with only the motion performance evaluated seems preferable to precise feedback control of every muscle length $\ell(t)$, or precise realization of torsion angle $\phi(t)$ by feedback control. That is the case especially in complex motions by a multi-DOF joint with highly parallel installation of StMAs. And then the relation between muscle contraction ξ and motor drive time t is much more convenient to use.

The actuator's basic control characteristics $\xi(t, T)$ is a formula expressing the contraction ξ of a muscle of natural length L under a constant muscle tension T generated by driving the motor for t[sec] with impressed voltage V_c. Note that L and V_c are usually fixed and omitted to show for simplicity. In the following sections the basic control characteristics $\xi(t, T)$ are used instead of $\xi(\phi, T)$.

3. Angle/Stiffness Control of StMA-based Joints

The control scheme for 1-DOF StMA-based joint and some experimental results are presented.

3.1 StMA-based joint

1-DOF joint rotation is realized by antagonistically installed two actuators (Fig.2, Fig.9). Use of a pulley as in Fig.2 makes the joint rotation angle θ linear to muscle contraction ξ, the analysis and control are then easy. But the flexibility of mechanical composition will be lost.

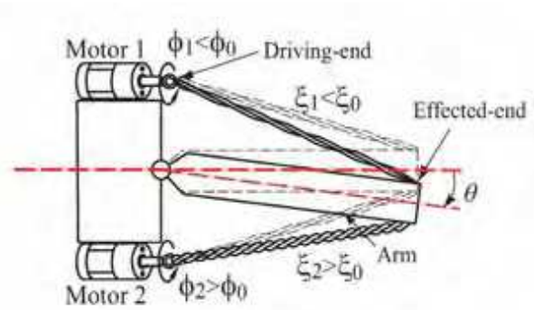

Fig. 9. A direct-connect-type StMA-based 1-DOF joint

Another type of actuator installation with its driving-end and effected-end directly connected as in Fig. 9. is suitable for constructing multi-DOF joints. A multi-DOF joint with high failure tolerance is realized by equipping several redundant actuators in parallel as in Fig. 10. Control of such multi-DOF joints is discussed in section 5.

With the antagonistic muscles the joint stiffness control is easy as well as joint angle control. In spite of simple structure the muscle itself functions as a speed reducer and a stiffness regulating mechanism. Hence downsizing and weight saving are easily achieved. The speed reduction ratio (gear ratio), ϕ/θ, depends mainly upon the muscle lengths, the muscle assignment and the pulley radius in case of a pulley-type joint. In addition the muscle tensions, or joint stiffness, also affect the ratio.

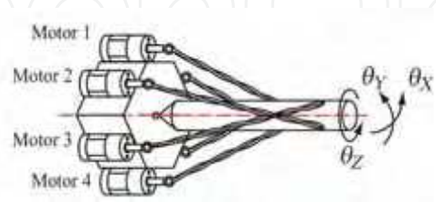

Fig. 10. An StMA-based 3-DOF joint with 6 StMAs

It is possible to select/increase muscles according to the actual use because the muscles are easy to equip and replace. This leads to another good feature: the joint characteristics can be easily improved, variable structure, or moreover, extendable joint mechanism might be possible.

3.2 Control of StMA-based Joints

StMA-based joints realize flexible and complex motions. On the other hand the mathematical model of the actuator is difficult to establish because of various non-linear factors to consider such as fiber bending moment, fiber surface friction and so on. When redundant actuators are installed on a multi-DOF joint and motions to realize become complex, the modeling is more difficult. It is necessary to utilize some additional learning technique, though StMAs are basically controlled based on the control equation derived from geometrical analysis with preliminary experiments.

Joint angle control Consider a joint in Fig.2 with two StMAs of the same material/radius /length muscles driven with the same motor voltage. In this case joint angle remains θ = 0 when $\xi_1 = \xi_2$, *i.e.*, $\phi_1 = \phi_2$ even if the muscles are twisted and tense (Fig.2(a)). When $\phi_1 \neq \phi_2$ contractions ξ_1, ξ_2 are different, and then the joint rotates (Fig.2(b)). The angle θ is determined by the linear geometric relation

$$\theta = \frac{\xi_1}{R} - \bar{\theta} = -\frac{\xi_2}{R} + \bar{\theta} \tag{5}$$

where R is the pulley radius, $\pm\bar{\theta}$ are the upper/lower bound of the operation ranges realized when muscle 1 or 2 is in natural state. Practically however, the geometric equation (5) needs to be compensated according to the experimental control result in order to improve control accuracy. The compensated equation is given in the form of $\theta = \frac{c_1 \xi(t,T)}{R} + c_2\bar{\theta} + c_3$, where $|c_1|, |c_2| \simeq 1, |c_3| << 1$.

In case of a direct-connect-type joint as shown in Fig.9 the angle θ is determined, in general, by a non-linear geometric relation

$$\theta = f(\xi_1) - \bar{\theta} = -f(\xi_2) + \bar{\theta} \tag{6}$$

where f is determined by the layout of actuator mounting, *i.e.*, position of driving/effected-ends of the muscles.

Both for linear and non-linear types, an StMA-based-joint angle control is achieved by realizing necessary muscle contractions ξ_1 and ξ_2 based on the basic control characteristics $\varepsilon(t,T)$. Fig.11 shows the relation between the drive time t and (imaginary) joint angles

θ_1, θ_2 when the muscles are separately set so that joint angles are $\theta_1 = -\bar{\theta}, \theta_2 = \bar{\theta}$ without muscle twist under a constant tension T. When actuator 1 is driven from an initial state

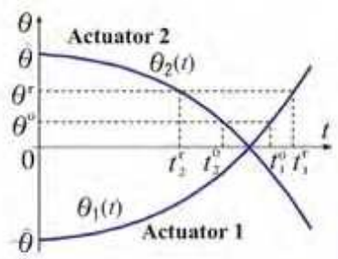

Fig. 11. Actuator state curves for joint angle control under constant tension

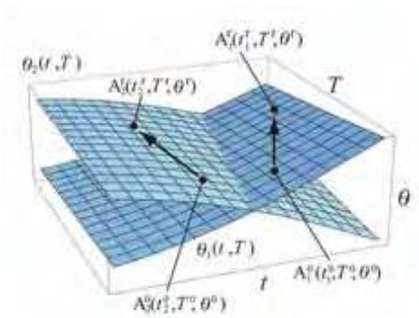

Fig. 12. Actuator state surfaces for joint angle/stiffness control

with keeping the tension T, the joint angle θ_1 changes along the curve $\theta_1(t) = \xi_1(t,T)/R - \bar{\theta}$. Such is the case also for the curve $\theta_2(t) = -\xi_2(t,T)/R + \bar{\theta}$. Actually, only states with $\theta = \theta_1(t_1) = \theta_2(t_2)$ are possible since the muscles are antagonistically connected to the common arm. Suppose that $\theta = \theta^0$ in the initial state. In order to realize joint angle θ^r the actuators are then driven for $t_1^r - t_1^0$ and $t_2^r - t_2^0$, respectively, where t_m^0, t_m^r are obtained as $t_m^0 = \theta_m^{-1}(\theta^0), t_m^r = \theta_m^{-1}(\theta^r), m = 1,2.$ ($t_m <$ 0 means drive in reverse direction for $|\, t_m \,|$)

Extending the curved lines in Fig.11 in terms of T, the actuator state surfaces in Fig.12 is obtained. At the points $\mathrm{A}_1^0, \mathrm{A}_2^0$ the muscles realize joint angle θ^0 under the tension T^0. In order to realize a desired state $\theta = \theta^r, T = T^r$ represented at A_1^r and A_2^r, the necessary drive times t_1 and t_2 are obtained from the target joint angle and muscle tension by the joint control equation

$$t_m = \theta_m^{-1}(\theta^r, T^r) - \theta_m^{-1}(\theta^0, T^0), m = 1,2 \quad (7)$$

The control result for $\bar{\theta} = 40$ [deg], $R = 16.5$ [mm] is shown in Fig.13 (left). The joint angle control with accuracy less than 2 [deg] is possible for a wide range of muscle tension.

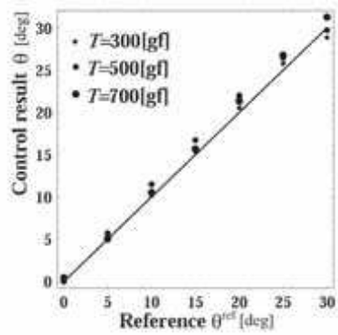

Fig. 13. Experimental result of joint angle control

Joint stiffness control The joint stiffness S_J is defined as

$$S_J = \frac{\partial M}{\partial \theta}$$

where M is the moment given to the joint which has a specified angle θ under a constant tension T. The result of stiffness control experiment is given in Fig.14 to show the wide controllable joint stiffness range.

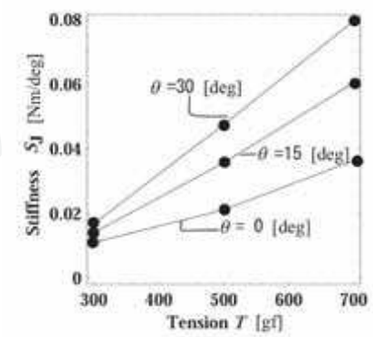

Fig. 14. Experimental result of joint stiffness control

The result says that the joint stiffness can be controlled through muscle tension control without joint angle change. As mentioned in subsection 2.2 the muscle is less stiff for larger torsion angle ϕ. Therefore an StMA for flexible, *i.e.*, soft joints needs longer muscle with larger initial torsion. The resultant joint angle/stiffness control had enough accuracy, and it was verified to be effective for hexapod walking.

4. Energy Efficient Walking of Legged Robots

In order for robots to perform dexterous behaviors in practical environments, quick actions such as fast walk and rapid turn with small energy cost are desired. The purpose of the work introduced in this section is thus realization of springy walk, *i.e.*, quick and energy-efficient rhythmical walk by StMA-based legged robots.

In the following a 6-legged StMA-based walking robot, SMAR-III, is introduced and the experimental result of walking is presented. A method for springy walk by actuator drive pattern optimization is presented and the prospect of fast and energy efficient walk is given.

4.1 StMA-based Walking Robot

Several StMA-based hexapod walking robots have already been made. SMAR-II (Fig.15, left) has 12 active joints, all ntagonistically driven by StMAs. The StMA's elastic property contributes to the walking ability in rough terrain. Small roughness is overcome without sensing. Another StMA-based robot, SRAMI (Fig.15, right), is a miniature size hexapod that swings each leg with a 2-DOF joint. SRAMI carries two 006P-9V batteries on the back and walk with the battery power. They walk but slow, and do not necessarily make the most of the StMA advantages.

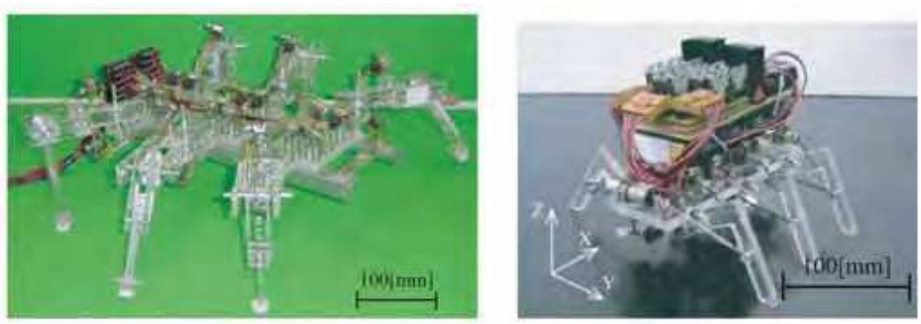

Fig. 15. StMA-based hexapod walking robots: SMAR-II (left) and SRAMI (right)

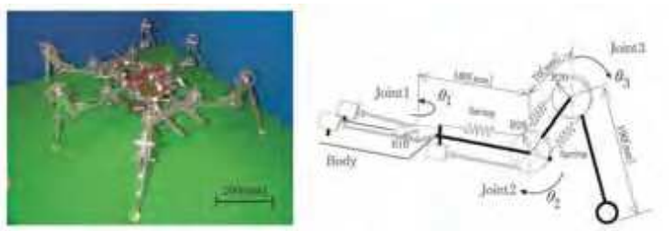

Fig. 16. StMA-based hexapod walking robot SMAR-III: Overview (left) and leg mechanism (right)

The SMAR-III (Fig.16) has 18 joints, 12 of which are driven by 18 StMAs. Each leg has three joints. Joint 1 and 2 are active 1-DOF joints, which are driven by antagonistic and semi-antagonistic StMAs, respectively. Joint 3 is a passive 1- DOF joint which contributes springy

Fig. 17. Tripod gait walking of SMAR-III

walk. Each StMA consists of a DC motor with reduction gear ratio 1/33 and PE-Line (polyester-twine fishing line) of ϕ = 0.5[mm] as muscle fibers. The size is 445 L×571W×195H[mm] in its basic posture, and the weight is 1.47 [kg] (without power supply, computer and cables). Every actuator is driven by a simple on/off control.

Walking is realized according to a predefined on/off actuator drive pattern based on the control equation. Straight tripod walk on a flat terrain has been realized and the captured motion is shown in Fig.17. The walking velocity is about 75 [mm/sec] that is much faster than 15 [mm/sec] by SMAR-II.

4.2 Energy efficient Springy Walk

It is true that the walking by SMAR-III is much faster than conventional, but it is still not so efficient. The simulated motion of θ_1 of the leg 1 (left foreleg) during walking is shown in Fig.18 (left). Without actuator drive pattern optimization in terms of energy efficiency and walking speed there remains an undesirable vibration after each stride (dotted ovals), i.e.,

time consuming body swinging without forward move. It makes walking velocity lower and wastes elastic energy.

Efficient and rhythmical walking is realized by utilizing the actuators' elasticity property and the inertia force by the motion. In other words, the energy efficient walking with a low-duty- ratio intermittent drive is realized by storing the elastic energy obtained from inertia force of each leg by leg-swinging during swing phase and inertia force of the body during support phase. The criterion function for optimal actuator drive is, for example, defines as

$$J(\boldsymbol{a}) = \frac{1}{d_w(t_w)} \left(\alpha \int_0^{t_w} \| \boldsymbol{V}(t) \|^2 dt + \beta t_w \right) \tag{8}$$

where $\boldsymbol{a}$ is the parameter vector that specifies actuator drive pattern such as walking cycle and on/off switching timing for each actuator, $\boldsymbol{V}(t)$is motor drive voltage vector, t_w is the walking time, $d_w(t_w)$ is the walking distance for t_w. The criterion is to minimize the energy consumption per unit walking distance (by the 1st term) and to maximize walking velocity (by the 2nd term).

The result of optimizing the drive pattern for joint 1 (Fig.18 right) says that the walking speed can be nearly doubled with less energy consumption. It was shown that springy walk based on the actuator drive pattern optimization technique will be possible. The optimization of the joint 1 motion realizes, as it were, rhythmical swinging walk and besides

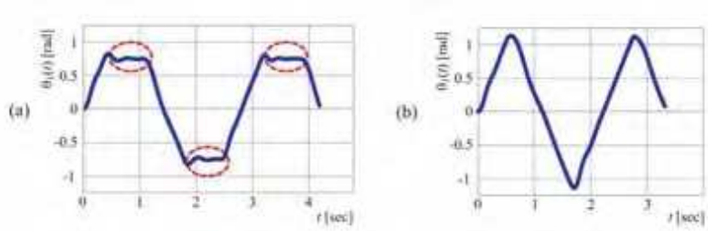

Fig. 18. Motion of joint 1 in (a) nonoptimal and (b) optimal actuator drive pattern

rhythmical hopping walk will be realized by optimizing the joint 2 motion.

5. Muscle Coordination of Multi-DOF Joints

General-purpose robotic manipulators with controllable joint stiffness like human arm joints are now desired. A human arm dexterously realizes complex motions by use of multi-DOF joints with redundant muscles. Although muscle coordination is essential for smooth motions and is an old problem, it is still an open problem (Latash & Turvey, 1996), and actively investigated in various fields (Yang et al., 2001,Tahara et al., 2005).

In this section the mechanism and control scheme for an StMA-based multi-DOF joint with redundant muscles are presented. An StMA-based robot arm is introduced first. Next a

muscle coordination method for StMA-based multi-DOF joint with redundant actuators is presented.

5.1 Strand-Muscle-Actuator-based Robot Arm

The StMA-based Robot Arm (StMA-RArm) is a robotic manipulator modeled on a human arm (Fig.19 left). It is composed of StMA-based Robot Shoulder (StMA-RS)(inside the dotted lines in Fig.20), a 1-DOF elbow (Joint 3), a 1-DOF wrist (Joint 4) and a simple 4-fingered hand. The mechanical composition is shown in Fig.20. The posture where the arm hangs down as in Fig.20 is referred to as the basic posture. It has 12 actuators at the StMARS, 2 at elbow, 4 at wrist-hand part, total 18 StMAs. DC geared motors of power rating 0.7[W] and 0.4[W], and Flyline of ϕ1.0[mm] and PE line of ϕ0.5[mm] for muscle fiber are used. For weight saving the fingers are controlled with 3 StMAs and auxiliary leaf springs. The size is 215W×194T×465H[mm], the weight is approximately 1.7[kg] (without controller circuits, computer, power supply).

Muscle vector *A muscle vector* is the vector from an effected-end to its corresponding driving-end (Fig.19 right). The muscle length is given by the norm of the muscle vector. For *n*-th actuator of Joint m to realize a desired posture $\boldsymbol{\theta}$ the muscle vector $\boldsymbol{\ell}_{mn}(\boldsymbol{\theta})$ is calculated from the coordinates of driving-end $\boldsymbol{P}_{\mathrm{E}mn}(\boldsymbol{\theta})$ and effected-end $\boldsymbol{P}_{\mathrm{D}mn}(\boldsymbol{\theta})$ as

$$\boldsymbol{\ell}_{mn}(\boldsymbol{\theta}) = \boldsymbol{P}_{\mathrm{D}mn}(\boldsymbol{\theta}) - \boldsymbol{P}_{\mathrm{E}mn}(\boldsymbol{\theta}), \qquad m = 1,2,3,4,\ n = 1,2,\cdots,N_m \tag{9}$$

where N_m is the number of actuators for Joint m. $\boldsymbol{P}_{\mathrm{E}mn}(\boldsymbol{\theta})$ and $\boldsymbol{P}_{\mathrm{D}mn}(\boldsymbol{\theta})$ are obtained from each effected/driving-ends $\boldsymbol{P}^{\,0}_{\mathrm{E}mn}$, $\boldsymbol{P}^{\,0}_{\mathrm{D}mn}$ in the basic posture by use of the

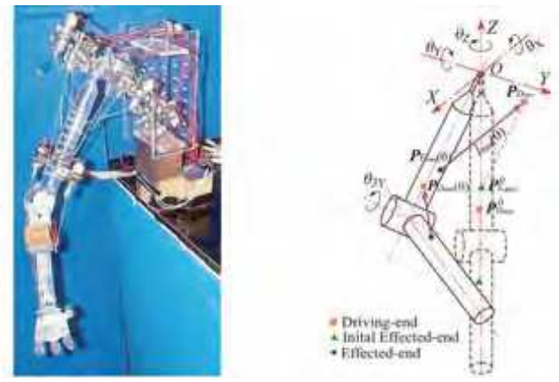

Fig. 19. StMA-RArm: Overview (left) and kinematic model of shoulder-elbow part (right)

rotational transformation matrix $\sum_m^H(\boldsymbol{\theta})$ as

$$\boldsymbol{P}_{\mathrm{D}mn}(\boldsymbol{\theta}) = \sum_m^H (\boldsymbol{\theta})\boldsymbol{P}_{\mathrm{D}mn}^0, \boldsymbol{P}_{\mathrm{E}mn}(\boldsymbol{\theta}) = \sum_m^H (\boldsymbol{\theta})\boldsymbol{P}_{\mathrm{E}mn}^0 \tag{10}$$

The necessary muscle contraction ξ_{mn} from the natural length L_{mn} is then

$$\xi_{mn}(\boldsymbol{\theta}) = L_{mn} - \|\boldsymbol{\ell}_{mn}(\boldsymbol{\theta})\|, \tag{11}$$

which is realized according to the StMA control method in section 3.

3-DOF Shoulder Parallel installation of StMAs easily realizes versatile multi-DOF joints. The StMA-RS is a human-shoulder-like high failure-tolerant 3-DOF joint with redundant muscles. It consists of Joint 1 (3-DOF) using a ball joint and Joint 2 (1-DOF). The motion ranges are $-20 \le \theta_{1X}, \theta_{1Y} \le 50[\mathrm{deg}], -60 \le \theta_{1Z} \le 60[\mathrm{deg}]$ for Joint 1, and $0 \le \theta_{2X} \le 30[\mathrm{deg}]$ for Joint 2. With cooperation of the two joints it achieves a large arm motion area. Both joints have redundant actuators, *i.e.*, 7 actuators $(A_{11} \sim A_{17})$ for Joint 1, and 5 actuators $(A_{21} \sim A_{25})$ for Joint 2. That contributes to the large capacity of joint stiffness control and failure tolerance. That is, wide range of joint stiffness can be realized for a wide variety of joint angle, and the motion of the joint can be easily recovered to some extent for some muscle breakage.

5.2 Control of 3-DOF Shoulder

Joint 1 and Joint 2 have a common center of rotation, therefore they can be regarded as a single 3-DOF joint with joint angle represented by $[\theta_X, \theta_Y, \theta_Z]$.

Muscle tension to resist external force Consider a 3-DOF joint driven by N StMAs. Let T_n be the tension generated by actuator n, and $\boldsymbol{T} = \{T_n\} \in \boldsymbol{R}^N$ be the tension vector composed of each actuator tension. An StMA generates tension in one direction only, and hence $T_n \ge 0$ always holds. The positive direction of $\boldsymbol{T}$ is the same as

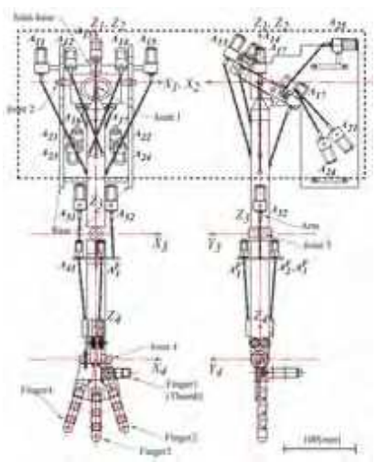

Fig. 20. Mechanism of StMA-RArm

that of the corresponding muscle vector. The moment $\boldsymbol{M} \in \boldsymbol{R}^3$ around the origin in posture $\boldsymbol{\theta}$ by the tension $\boldsymbol{T}$ is then given as

$$\boldsymbol{M} = \boldsymbol{H}(\boldsymbol{\theta})\boldsymbol{T} \tag{12}$$

where $\boldsymbol{H}(\boldsymbol{\theta}) \in \boldsymbol{R}^{3\times N}$ is given as

$$\boldsymbol{H}(\boldsymbol{\theta}) = \left[\boldsymbol{h}_1(\boldsymbol{\theta}) \;\; \boldsymbol{h}_2(\boldsymbol{\theta}) \;\; \cdots \;\; \boldsymbol{h}_N(\boldsymbol{\theta})\right] \tag{13}$$

$$\boldsymbol{h}_n(\boldsymbol{\theta}) = P_{\mathrm{En}}(\boldsymbol{\theta}) \times \boldsymbol{u}_n(\boldsymbol{\theta}), n = 1, 2, \cdots, N \tag{14}$$

$$\boldsymbol{u}_n(\boldsymbol{\theta}) = \frac{\boldsymbol{\ell}_n(\boldsymbol{\theta})}{\|\boldsymbol{\ell}_n(\boldsymbol{\theta})\|} \in \boldsymbol{R}^3, \; n = 1, 2, \cdots, N \tag{15}$$

Conversely the tension needed to keep the posture $\boldsymbol{\theta}$ under an external moment $\boldsymbol{M}$ is given as the general solution of (12) as

$$\boldsymbol{T} = \boldsymbol{H}^{\#}(\boldsymbol{\theta})\boldsymbol{M} + (\boldsymbol{I}_N - \boldsymbol{H}^{\#}(\boldsymbol{\theta})\boldsymbol{H}(\boldsymbol{\theta}))\boldsymbol{\beta} \tag{16}$$

where $\boldsymbol{H}^{\#}(\boldsymbol{\theta}) \in \boldsymbol{R}^{N\times 3}$ is the pseudo-inverse of $\boldsymbol{H}(\boldsymbol{\theta}), \boldsymbol{I}_N \in \boldsymbol{R}^{N\times N}$ is identity matrix and $\boldsymbol{\beta} \in \boldsymbol{R}^N$ is an arbitrary vector. Note that the 2nd term of the right side of (16) does not affect joint torque. The joint stiffness can be controlled by adjusting the tension $\boldsymbol{T}$, within $T_n \geq 0$, by use of $\boldsymbol{\beta}$

Angle control experiments The experimental Joint 1 angle control result of X-axis and Y -axis rotation for $0 \leq \theta_X, \theta_Y \leq 50[\mathrm{deg}]$ with $\boldsymbol{M} = 0$ and $\boldsymbol{\beta} = (100\,100 \cdots 100)^T$ are shown in Fig.21. Experiments show good angle control result for both θ_X and θ_Y for angles less than $40[\mathrm{deg}]$.

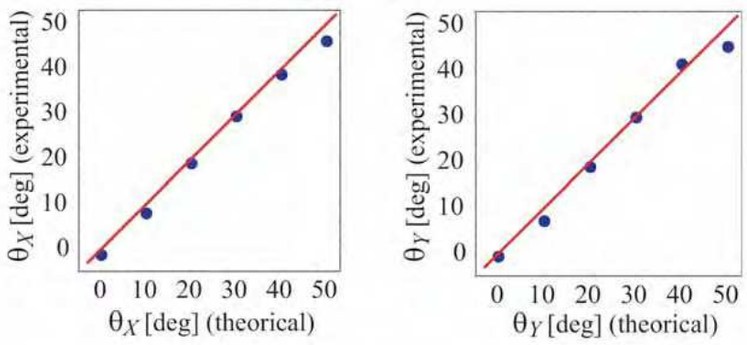

Fig. 21. Result of Joint1 angle control for X-axis rotation (left) and Y -axis rotation (right)

6. Optimal Redundant Muscle Coordination

The StMA-RArm realizes versatile flexible motions with StMA-RS. On the other hand the muscle tension combination to realize a specific task is not unique because of the redundant muscles. In order to realize complex tasks in practical environment, online optimal muscle tension combination adapting to varying situation is necessary because offline target tension setting is impossible.

In this section the method given in section 5 is applied to the online optimal muscle coordination for StMA-RS. As an optimization technique Particle Swarm Optimization (PSO) (Kennedy & Eberhart, 2001) is used with modification so that it keeps the suboptimal solution set in the steady state to adapt to time-variant objective function. The method realizes not only desired joint angle but keeping adequate joint stiffness and actuator load averaging all at the same time by optimal combination of muscle tension. In the following a method of online redundant muscle coordination by use of Vibrant Particle Swarm Optimization is presented, and some numerical experiments are given.

6.1 Optimal Cooperative Control of Redundant Muscles

The muscle tension combination to keep a certain posture is not unique because of the arbitrary vector $\boldsymbol{\beta}$ in (16). Therefore the tension combination for the robot arm with redundant muscles should be optimized for an adequate performance criterion. The optimal tension here means, for example, the state that keeps adequate joint stiffness without exerting excessive tension on partial muscles. For practical use the time trajectory of $\boldsymbol{\beta}$ (t) must be optimized for desirable muscle cooperation for all t with keeping specified joint angle $\boldsymbol{\theta}$ (t), and torque $\boldsymbol{M}$ (t). In other words, an optimization problem for a time variant object function must be solved. Consider the following problem to obtain the optimal tension combination by optimizing the arbitrary vector $\boldsymbol{\beta}$.

$$\boldsymbol{P}_T(t): \min_{\boldsymbol{\beta}(t)} J(\boldsymbol{\beta}(t)) = c_1 f_v(\boldsymbol{T}(\boldsymbol{\beta}(t))) + \frac{c_2}{N}\left\|\boldsymbol{T}(\boldsymbol{\beta}(t)) - \boldsymbol{T}^r(t)\right\|$$
$$\text{subj. to} \quad \boldsymbol{T}(\boldsymbol{\beta}(t)) \geq 0$$

where $\boldsymbol{T}(\boldsymbol{\beta}(t))$ is obtained from (9),(10),(13)~(16). f_v is standard deviation. $\boldsymbol{T}^r(t)$ is a target muscle tension distribution, $c_1, c_2 > 0$ are weighting coefficients. The first term in the criterion function aims at minimization of tension variation, the second term seeks realization of desirable tension distribution corresponding to given tasks. c_1 should be larger to prevent tension concentration, and c_2 should be larger when the realization of target tension is more important. The latter is the case, when different kinds of muscles are used for a joint and each muscle has different maximum allowable tension, for example.

6.2 Vibrant PSO For Time-variant Optimization

Consider a time-variant optimization problem $\boldsymbol{P}(t)$ formulated as

$$\boldsymbol{P}(t): \min_{\boldsymbol{x}(t)} f(t, \boldsymbol{x}(t)) \tag{17}$$

$$\text{subj. to } \boldsymbol{x}(t) \in \boldsymbol{G} \tag{18}$$

where $\boldsymbol{x}(t) = \{\boldsymbol{x}_n(t)\} \in R^N$ and (18) is upper/lower bounds constraints.

Consider to use the Particle Swarm Optimization (PSO) to solve $P(t)$. PSO is a form of swarm intelligence, and is vigorously investigated as a powerful multi-agent type optimization technique (Kennedy & Eberhart, 2001). PSO is modeled by particles in multi-dimensional space that have a position and a velocity. Based on their memory of their own best position and knowledge of the swarm's best position the particles (*i.e.*, the agents) adjust their own velocity and move through the search space to search the optimum.

In the canonical PSO many agents $\{\boldsymbol{x}_i\}$ (particles) are scattered in the search domain. Each agent searches the optimum using the following three kinds of information: (a) speed of the agent represented in discrete form by $\Delta \boldsymbol{x}_i$, (b) *personal best*: the best performance point realized by the agent, so-called pbest, represented by $\boldsymbol{x}_i^{pb}$, and (c) *global best*: the best performance point realized by all the agents, so-called gbest, represented by $\boldsymbol{x}^{gb}$. Movement of each agent (search point) is then given by

$$\boldsymbol{x}_i^{k+1} = \boldsymbol{x}_i^{k+1} + \Delta \boldsymbol{x}_i^k \tag{19}$$

$$\Delta \boldsymbol{x}_i^k = v_1 + v_2 + v_3 = w \Delta \boldsymbol{x}_i^{k-1} + c_p r_p (\boldsymbol{x}_i^{pb} - \boldsymbol{x}_i^k) + c_g r_g (\boldsymbol{x}^{gb} - \boldsymbol{x}_i^k) \tag{20}$$

where $\boldsymbol{x}_i^k$ represents $\boldsymbol{x}_i(k\Delta t)$ for $i = 1,2,\cdots,n_p; k = 0,1,2,\cdots,$ and $w, c_p, c_g > 0$ are weighting coefficients, $0 < r_p r_g < 1$ are random numbers. v_1, v_2, v_3 in (20) correspond to (a), (b), (c), respectively.

It is expected that the steady-state swarm of PSO holds the time-variant optimum $\boldsymbol{x}^*(t)$. The canonical PSO is, however, inapplicable to time-variant optimization as it is. Therefore the canonical PSO is modified by introducing 1) inter-agent distance control, and 2) agent variety maintenance. The modified PSO is referred to as Vibrant PSO (Vi-PSO) (Suzuki & Mayahara, 2007).

Inter-agent distance control By adding a vector v_4 to (20) to prevent convergence to x^{gb}, the PSO is made vibrant:

$$\Delta \boldsymbol{x}_i^k = v_1 + v_2 + v_3 + v_4 \tag{21}$$

$$v_4 = \frac{c_d}{(c_e \left\| \boldsymbol{x}^{gb} - \boldsymbol{x}_i^k \right\| + 1)^{\alpha}} \cdot \frac{\boldsymbol{x}^{gb} - \boldsymbol{x}_i^k}{\left\| \boldsymbol{x}^{gb} - \boldsymbol{x}_i^k \right\|} \tag{22}$$

where $c_d, c_e > 0, \alpha > 1$. If $\boldsymbol{x}^{gb} - \boldsymbol{x}_i^k \simeq 0$, an adequate unit vector generated by randomization is used instead. And in the Vi-PSO the search domain is normalized because the size of the domain affects the optimization through the use of the distance between an agent and $\boldsymbol{x}^{gb}$ in (22).

Agent variety maintenance As optimization progresses the distribution of agents becomes uneven, which often hinders optimum tracking. Hence some agents are probabilistically erased and new agents are produced at each time step. This selection/production reduces the uneven distribution, and increases the variety of agents. The Vi-PSO keeps suboptimal agents in steady state by adapting to the time varying object function by continuously searching near the current optimum.

6.3 Muscle Tension Optimization for StMA-RS

Problem setting The Vi-PSO is applied to problem $\boldsymbol{P}_T(t)$ in subsection 6.1, which is a muscle tension optimization for the StMA-RS control to adequately determine β for all *t* in control period.

Consider here to determine the muscle tension trajectory $\boldsymbol{T}(t) = \{T_i(t)\} \in \boldsymbol{R}^7$ in the case of controlling the joint angle θ_y continuously from $-15[°]$ to $15[°]$ in $0 \le t \le 10$ with moment around *y*-axis, *My* = 100, exerted (Fig.22).

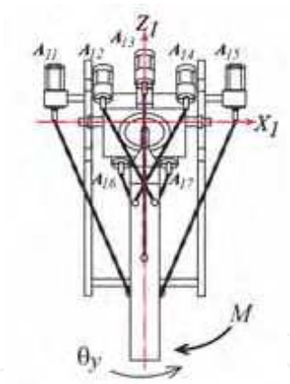

Fig. 22. StMA-based shoulder control problem: *y*-axis rotation under external moment

That is, the problem $\boldsymbol{P}_T(t)$ with the following specification in (16) is considered.

$$\boldsymbol{\theta}(t) = \begin{bmatrix} \theta_x \\ \theta_y \\ \theta_z \end{bmatrix} = \begin{bmatrix} 0 \\ 3t - 15 \\ 0 \end{bmatrix}, \quad \boldsymbol{M}(t) = \begin{bmatrix} 0 \\ 100 \\ 0 \end{bmatrix} \tag{23}$$

To prevent unrealistic elongation force (repulsive force between driving-end and effectedend), that is, to keep $T_i \geq 0$, a penalty function was added to the object function. The parameters used are $c_1 = 1, c_2 = 1, \boldsymbol{T}^r = (100, 100, \cdots, 100)^T \in \boldsymbol{R}^7$ in object function, $w = 0.9, c_p = 0.1, c_g = 0.01, c_d = 0.25, c_e = 20, \alpha = 4$ in Vi-PSO. And the positions of driving/effected-ends of the StMA-RS in the basic posture are

$$
\begin{aligned}
A_{11}: \quad & \boldsymbol{P}^0_{\mathrm{D}11} = (-65, 0, -30), && \boldsymbol{P}^0_{\mathrm{E}11} = (-12.5, 0, -180) \\
A_{12}: \quad & \boldsymbol{P}^0_{\mathrm{D}12} = (-40, 55, 5), && \boldsymbol{P}^0_{\mathrm{E}12} = (8.8, -8.8, -80) \\
A_{13}: \quad & \boldsymbol{P}^0_{\mathrm{D}13} = (0, 60, 30), && \boldsymbol{P}^0_{\mathrm{E}13} = (0, 12.5, -145) \\
A_{14}: \quad & \boldsymbol{P}^0_{\mathrm{D}14} = (40, 55, 5), && \boldsymbol{P}^0_{\mathrm{E}14} = (-8.8, -8.8, -80) \\
A_{15}: \quad & \boldsymbol{P}^0_{\mathrm{D}15} = (65, 0, -30), && \boldsymbol{P}^0_{\mathrm{E}15} = (12.5, 0, -180) \\
A_{16}: \quad & \boldsymbol{P}^0_{\mathrm{D}16} = (-35, -35, -64), && \boldsymbol{P}^0_{\mathrm{E}16} = (8.8, 8.8, -140) \\
A_{17}: \quad & \boldsymbol{P}^0_{\mathrm{D}17} = (35, -35, -64), && \boldsymbol{P}^0_{\mathrm{E}17} = (-8.8, 8.8, -140)
\end{aligned}
$$

Optimization result Optimization results are shown in Fig.23 and 24. The time charts of $\boldsymbol{\beta}(t)$ and $\boldsymbol{T}(t)$ are shown in Fig.23. Note that $\boldsymbol{T}(t)$ was calculated using (16) with $\boldsymbol{\beta}(t)$, and

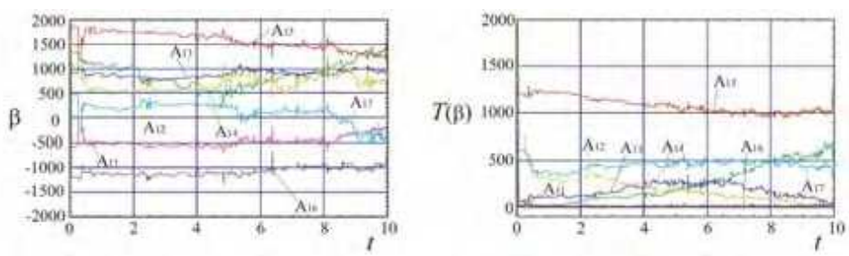

Fig. 23. Transition of muscle tension optimzing vector β and resultant muscle tension

hence the resultant $\boldsymbol{T}(t)$ always realizes the target joint angle $\boldsymbol{\theta}(t)$ and moment $\boldsymbol{M}(t)$. Muscle tensions waved bitterly at the initial stage of the optimization, but as optimization progresses, the movement settled down. The tension was concentrated to A_{15} which can generate *y*-axis moment efficiently. Most tensions were larger than the target tension $T_i^r = 100$ because the target was much smaller than the necessary ones to resist $\boldsymbol{M}(t)$. Therefore the second term in the objective function in this case worked to minimize muscle tensions.

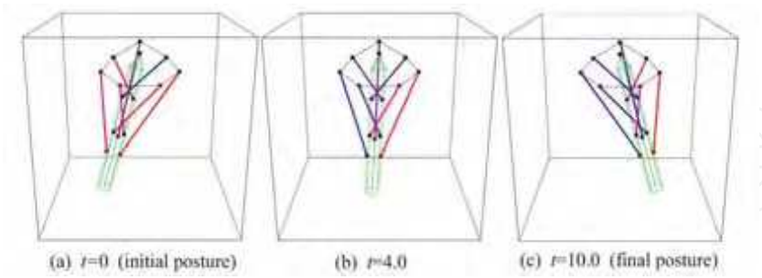

Fig. 24. Transition of posture and muscle tension

Fig.24 visually shows the posture and muscle tension transition. A muscle is colored red when its tension is large, blue when small. Except the initial state (a), where optimization does not progress yet, right side muscles have mainly large (red) tensions to resist the external moment. On the other hand left side ones have small (blue) ones, especially in later state, because no large tension is necessary for the requested motion.

Smoothing for practical use In Vi-PSO the optimal solution moves jumping from one point to another, therefore optimal $\boldsymbol{\beta}$ and corresponding muscle tension show non-smooth transition as in Fig.23, and so inadequate to use for control as it is. For practical use it is necessary to smooth the tension transition, for example by filtering the transition. Fig.25 shows the smoothed $\boldsymbol{\beta}$ and corresponding muscle tension.

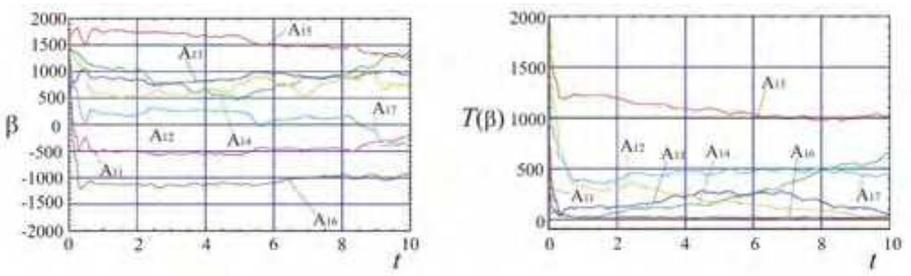

Fig. 25. Transition of smoothed $\boldsymbol{\beta}$ and corresponding muscle tension $(c_1 = 1, c_2 = 1)$

It should be noted that the smoothed tension $\boldsymbol{T}(t)$ strictly realizes the target joint angle $\boldsymbol{\theta}(t)$ for $\boldsymbol{M}(t)$, although the smoothed $\boldsymbol{\beta}$ is not strictly optimal for the criterion.

Modifications depending on circumstances In order to adapt to task environment the object function is modified depending upon the circumstances.

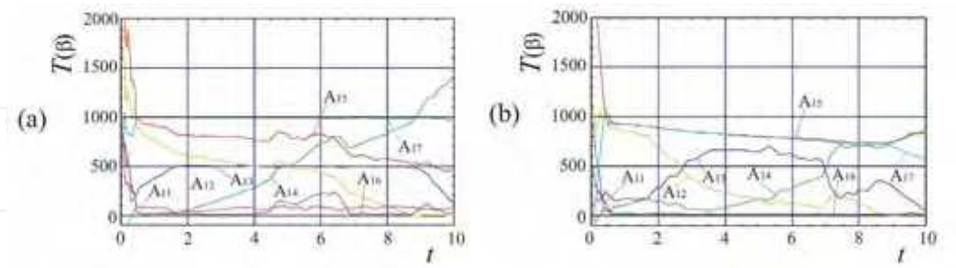

Fig. 26. Transition of muscle tension for modified criterions

Fig.26(a) shows the optimization result for $\boldsymbol{P}_{\boldsymbol{T}}(t)$ with altered object function parameters $c_1 = 0.1, c_2 = 1$ and $\boldsymbol{T}^r = (100, 500, 500, 500, 100, 1000, 1000)^T$ Comparing to the result in Fig.25 a smaller weight c_1 to evaluate muscle tension distribution minimization was used. As a result large tensions were permitted for strong muscles like A_{14} and A_{17}, the tension for weak A_{15} was restrained, and some muscles exert near targeted tensions. Fig.26(b) shows the optimization result for a min-max criterion: $J(\boldsymbol{\beta}(t)) = \max_n \{T_n(\boldsymbol{\beta}(t))\}$, which shows a smooth transition of the maximum muscle tension. The maximum tension was minimized as intended, *i.e.*, much smaller than the counterparts in Figs.25 and 26(a), which will contribute to lessen the possibility of muscle failure. The result says that adequate muscle coordination control according to situation change was successfully realized.

The real-time muscle coordination control of redundant muscles by use of Vibrant PSO was presented and shown to be effective for 3-DOF StMA-based joint motion control with considering optimal muscle tension distribution. With the target muscle tension $\boldsymbol{T}(t)$ obtained by solving $\boldsymbol{P}_{\boldsymbol{T}}(t)$ and the necessary contraction of each muscle obtained from joint angle θ *(t)* by use of (9) and (11), an StMA-based robot is controlled based on the basic characteristics.

7. Discussions

Towards biped walking humanoid Development of humanoid robots is increasingly active. A biped walking mechanism using StMAs is now under development. The muscle coordination in multi-DOF joints and its online optimal control presented in sections 5 and 6 are applicable not only to shoulder control, but also to any multi-DOF joints such as wrists, hip joints, ankles and neck, or even to eyes and tongue movement.

The StMAs are small, light and simple. They are suitable for application to robotic hands, in which many actuators must be installed in the palm or in the forearm. The StMAbased hand in Fig.27 has 20 StMAs installed at the forearm, and the tension is transferred to wrist and fingers through tendon sheaths. 12 actuators are used as finger flexor muscles with leaf springs used as the corresponding extensor muscles. Leaf springs are also useful as the base

for force sensor with strain gauges. The hand in fact can measure the weight of grasping objects with a strain-gauge-based force sensor at the wrist.

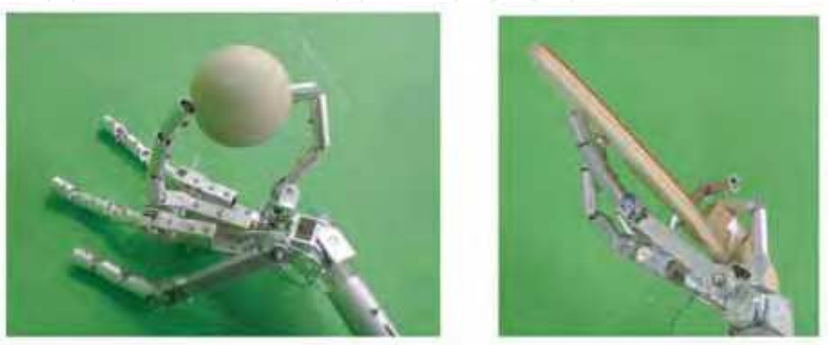

Fig. 27. StMA-based 5-fingered hand pinching a ping-pong ball and gripping a ping-pong racket

For practical utilization more investigation on the strand muscle itself, especially muscle fiber, and motor might be necessary. A strand muscle should be composed not by using handy materials, but by elaborately designed muscle fibers. More compact motors such as ultrasonic motors, or some innovative motors will drastically extend the StMA's applicability.

For autonomous realization of complex tasks A humanoid robot has so many joints. From the practical point of view, it seems almost impossible to precisely plan/specify all the joint motions in a top-down manner. An action planning/control strategy generated in a bottom-up manner with some hierarchical structure is inevitable. It is especially the case for StMA-based robots, each of whose joints is driven by two or more actuators.

The authors are researching an evolutionary behavior learning methodology with a hierarchical structure: Intelligent Composite Motion Control, ICMC (Suzuki, 2000), and applying it to robot behavior realization (Suzuki et al., 2001). The ICMC aims for realizing intelligent robots that can realize complex behaviors adaptively just by giving them the motion control for fundamental element motions. Starting from fundamental motions, complex behaviours are gradually realized by successive learning. In order to realize truly intelligent robots that flexibly and dexterously accomplish complex tasks like the human in the future, the behaviour realization must not be just an ad hoc execution but should be an acquisition with large capabilities. The ICMC gives a systematic behavior acquisition method by building up a capacious action intelligence network called the knowledge array network, which adaptively grows step-by-step in an evolutionary manner (Suzuki, 2005). The future work on the StMAs therefore includes the application of the methods presented in this chapter to practical tasks based on the ICMC.

8. References

Kennedy, J.; Eberhart, R. C. (2001). Swarm Intelligence, Morgan Kaufmann

Latash, M. L.; Turvey, M. T. (1996), Dexterity And Its Development, Lawrence Erlbaum Associates Publishers

Linde, R. Q. van der (1999), Design, analysis, and control of a low power joint for walking robots, by phasic activation of McKibben muscles, IEEE T. Robotics and Automation, Vol. 15, No. 4, pp.599-604

Suzuki, M.; Akiba, H.; Ishizaka, A. (1997), Strand-muscle robotic joint actuators (in Japanese), Proc. 15th RSJ Annual Conf., pp.1057-1058

Suzuki, M. (2000), A method of robot behavior evolution based on Intelligent Composite Motion Control, Journal of Robotics and Mechatronics, Vol.12, No.3, pp.202-208

Suzuki, M.; Scholl, K.-U.; Dillmann, R. (2001), Complex and dexterous soccer behaviours based on the Intelligent Composite Motion Control, Proc. 4th Int. Conference on Climbing and Walking Robots, Karlsruhe, pp.443-450

Suzuki, M.; Ichikawa, A. (2004), Toward springy robot walk using Strand-muscle actuators, Proc. 7th Int. Conf. Climbing&Walking Robots, pp.467-474, Madrid

Suzuki, M. (2005), Evolutionary acquisition of complex behaviors through Intelligent Composite Motion Control, Proc. 6th IEEE Int. Symp. Computat. Intelligence in Robotics and Automation, Espoo

Suzuki, M.; Mayahaya, T. (2007), Optimal Muscle Coordination of A Robot Joint using Vibrant Particle Swarm Optimization, Proc. 13th IASTED Int. Conf. Robotics and Applications, Wuerzburg, to appear

Tahara, K. et al. (2005), Sensory-motor control of a muscle redundant arm for reaching movements – convergence analysis and gravity compensation, Pros. 2005 IEEE/RSJ Int. Conf. on Intelligent Robots and Systems (IROS 2005), pp.517-522

Yang, N. F. et al. (2001), A function description for the human upper limb pointing movements performance, Proc. 23rd Annual Int. Conf. IEEE Engineer. in Medicine and Biology Society, Vol.2, pp.1236-1239

Proc. 2nd Conf. on Artificial Muscles (2004), Ikeda, Japan

Climbing and Walking Robots: towards New Applications
Edited by Houxiang Zhang

ISBN 978-3-902613-16-5
Hard cover, 546 pages
Publisher I-Tech Education and Publishing
Published online 01, October, 2007
Published in print edition October, 2007

With the advancement of technology, new exciting approaches enable us to render mobile robotic systems more versatile, robust and cost-efficient. Some researchers combine climbing and walking techniques with a modular approach, a reconfigurable approach, or a swarm approach to realize novel prototypes as flexible mobile robotic platforms featuring all necessary locomotion capabilities. The purpose of this book is to provide an overview of the latest wide-range achievements in climbing and walking robotic technology to researchers, scientists, and engineers throughout the world. Different aspects including control simulation, locomotion realization, methodology, and system integration are presented from the scientific and from the technical point of view. This book consists of two main parts, one dealing with walking robots, the second with climbing robots. The content is also grouped by theoretical research and applicative realization. Every chapter offers a considerable amount of interesting and useful information.

How to reference
In order to correctly reference this scholarly work, feel free to copy and paste the following:

Masakazu Suzuki (2007). Complex and Flexible Robot Motions by Strand-Muscle Actuators, Climbing and Walking Robots: towards New Applications, Houxiang Zhang (Ed.), ISBN: 978-3-902613-16-5, InTech, Available from: http://www.intechopen.com/books/climbing_and_walking_robots_towards_new_applications/complex_and_flexible_robot_motions_by_strand-muscle_actuators

INTECH
open science | open minds

InTech Europe
University Campus STeP Ri
Slavka Krautzeka 83/A
51000 Rijeka, Croatia
Phone: +385 (51) 770 447
Fax: +385 (51) 686 166
www.intechopen.com

InTech China
Unit 405, Office Block, Hotel Equatorial Shanghai
No.65, Yan An Road (West), Shanghai, 200040, China
中国上海市延安西路65号上海国际贵都大饭店办公楼405单元
Phone: +86-21-62489820
Fax: +86-21-62489821

IntechOpen